IET Generation, Transmission & Distribution

Research Article

IET Journals
The Institution of Engineering and Technology

Wind power converters improving the power system stability

ISSN 1751-8687
Received on 17th July 2015
Revised on 28th October 2015
Accepted on 17th December 2015
doi: 10.1049/iet-gtd.2015.0889
www.ietdl.org

Andres E. Leon[1] ✉, Gustavo Revel[1], Diego M. Alonso[1], Guillermo E. Alonso[2]

[1]*Instituto de Investigaciones en Ingeniería Eléctrica (IIIE)' Alfredo Desages' (UNS-CONICET), Universidad Nacional del Sur (DIEC-UNS), Avda. Alem 1253, Bahía Blanca 8000, Argentina*
[2]*Electrical Engineering Consulting Services, ICONO s.r.l, Bahía Blanca 8000, Argentina*
✉ *E-mail: aleon@iiie-conicet.gob.ar*

Abstract: This study analyses the coordinated actions of modern wind power plants for improving the transient and small-signal stability in power systems. Supplementary controls on wind farms are considered, and specific modifications on the controllers are tailored to increase the grid-support services. The proposal is analysed and validated in a practical power system based on the Argentine electrical network. The wind farm supplementary controls use active and reactive power control loops as well as local and remote measurements. Local controls can rapidly respond decelerating the system frequency in the first instants of a fault, consequently reducing the transient angle separations and improving the first-swing stability. On the other hand, remote controls using global information are able to increase the damping of low-frequency inter-area oscillations. Structures combining centralised and decentralised control approaches will become more common in the near future. With this aim, the integration of fast local controls with remote controls is thoroughly studied using non-linear time-domain simulations and eigenvalue analyses. A robustness evaluation is also performed to validate the proposal over a wide range of operating conditions.

1 Introduction

The integration of large amounts of renewable energy generation into the electric grid and the continuous increase in power demand pose challenges to the transmission infrastructure planning and operation [1–3]. At the same time, most of the renewable sources are connected to the grid through power electronic devices, introducing a higher flexibility for power control and enabling the inclusion of additional grid-support services [4]. Several control strategies using the power electronic converters of modern variable-speed wind turbines for transient stability improvement [5], inter-area oscillation damping [6], voltage support [7], and short-term frequency regulation [8] were proposed in the last decade. Additional benefits can arise when the simultaneous actions of supplementary services combining centralised and distributed controls are further explored. It is interesting the application of these additional support tasks in large power systems where the high-quality wind resources are geographically far from load centres and connected to weak buses, in particular, where large-scale wind farms and long-distance transmission lines are under construction or being projected. These lines often include series compensation based on fixed capacitors with the objective of increasing the power transmission capacity, decreasing losses by power sharing between parallel lines, and reducing steady-state and transient angle separations among bus voltages [9, 10]. The compensation level is usually selected (with some conservativeness) to improve the transient stability margin and the fault-tolerance capability, but increasing the risk of triggering subsynchronous interactions with thermal and wind power plants [11–15]. On the other hand, transient stability can be enhanced by the wind power converters tailoring their local controls. Several wind farms can also be coordinated by means of centralised controls [16] that process remote data from distributed phasor measurement units (PMUs) [17–19], in order to improve the small-signal stability.

In this work, the coordinated action of modern wind farm control strategies is used to enhance the transient and small-signal stability in a case study based on the Argentine power system. This system presents many long-distance transmission lines with fixed series compensation, thermal power units prone to undergo subsynchronous resonance (SSR), and large areas of wind generation far from the main load centres (more than 1000 km) [20]. To achieve the proposed objective, a supplementary control scheme for wind power converters is designed combining different approaches which have recently appeared in the literature, and are conveniently modified to improve the system stability. The dedicated supplementary controls are arranged in two levels. The first one consists of local controls, including a transient power modulator and the reactive current injection during fault conditions. The local controls can rapidly respond after a fault, decelerating the system frequency, reducing the transient angle separations, and improving the first-swing stability. The second level is a remote (or centralised) control that uses global measurements from wide-area measurement systems (WAMS) to increase the damping of low-frequency inter-area modes, complementing the first level actions and improving the small-signal stability. The effect on transient and small-signal stability of each individual control loop, as well as the combined action of the whole strategy, is analysed in detail using non-linear time-domain simulations and eigenvalue analyses. The proposed approach of including the wind farm supplementary controls is compared with a conventional method for improving the transient stability by means of increasing the series compensation level. A robustness assessment is also performed to validate the study over a wide range of operating conditions, including several line outages and different load dispatches.

2 Test system

The studied system is derived from one of the future scenarios of the Argentine power system considered by the transmission system operator. This case study includes several projected large-scale wind farms and new long-distance corridors. Several features, such as large areas of high-quality wind generation far from the main load centres and long-distance corridors (most of them including

fixed series compensation) make this system useful for the evaluation of the coordinated control action of wind power converters. The power system model consists of 212 buses, 43 synchronous generators, and 18 wind farms. A simplified single-line diagram of the electrical network is shown in Fig. 1. Some key features of the system are (i) approximately 40% of the power demand is concentrated in the GBA area; (ii) the areas Comahue and GBA are connected through corridors transporting more than 5000 MW using 500 kV ac lines with a longitude of 1200 km and 50% of fixed series compensation; (iii) the thermal power plant at bus 2000 (see Fig. 1) is prone to undergo SSR; (iv) more than 3000 MW of wind generation is projected in the Patagonia region, where the wind power densities and capacity factors are among the best in the world; (v) the power flow in the Patagonia corridor (1500 km from bus 19 to 1008) will be based mostly on wind farms, and the wind power will be transported through series capacitor compensated lines; and (vi) the buses in the Patagonia region have low short-circuit power; therefore, power plants in this region are vulnerable to transient stability problems.

In this study, the synchronous generators are represented by two-axis models with the corresponding automatic voltage regulators (IEEE-ST1A) and power system stabilisers (IEEE-PSS1A) [21]. The network transmission lines are represented using equivalent π circuits. The parameters of both the machines and the electrical network are extracted from the reference guide of the Argentine transmission system operator. The key parameters of the system are included in the Appendix.

The wind farms are represented by aggregated models consisting of a permanent-magnet generator with full-power converters and a two-mass drive-train system [22, 23]. The wind farm control strategy, shown in the schematic diagram of Fig. 2, includes standard and supplementary controls. The standard ones consist of the maximum power point tracker (MPPT) and the voltage regulator blocks (dark grey blocks). The MPPT block extracts the maximum power available from the wind [23], and the voltage regulator adjusts the terminal voltage in steady state. The latter is performed by a proportional–integral (PI) control with a droop of 5% [24]. On the other hand, the supplementary controls can be divided into local and remote blocks and will be described in detail in Section 3.

The main power system electromechanical modes below 1 Hz (without considering the supplementary controls) are shown in Table 1, where a modal analysis is presented. Note that various of these modes are poorly damped, with damping ratios lower than 10%. The small-signal analysis and the non-linear time-domain simulations are performed using the MATLAB® 2014a software.

3 Wind farm supplementary controls

This section describes the dedicated supplementary actions combined with the wind farm control strategy to improve the system performance. The low voltage ride-through (LVRT) characteristic of the wind power converters is modified to increase the voltage support during faults, and a transient power modulator (TPM) is designed to decelerate the system frequency immediately after a severe disturbance. These types of controllers are currently considered for wind power converters, but in this work, they are tailored to further improve the transient stability of the system. In the case study, all the wind farms include these control blocks. In addition, in selected wind farms, a remote control action is introduced to provide extra damping to low-frequency inter-area modes.

3.1 Local control blocks

Both the LVRT and TPM blocks use local measurements to compute additional terms for the reactive and active power references, respectively.

The LVRT block is able to quickly respond during fault conditions, injecting the additional reactive current required by the grid codes. This reactive current is specified by the current/voltage curve (shown in Fig. 2) with a slope k, called 'reactive slope' in the following paragraphs. For example, a reactive slope $k = \Delta I/\Delta V = 2$ (German grid code) means that, when the voltage drops below 0.5 pu, the wind farm has to inject its nominal reactive current [25]. To improve the first-swing stability, the reactive slope is raised to $k = 4$, increasing the voltage support from wind power plants during faults. Thus, immediately after a fault event, the conventional power plants can increase the delivered active power, avoiding excessive rotor angle separations and improving the transient stability.

The TPM operates so that when the frequency at the wind farm bus is below its nominal value, the wind farm increases the active power injected into the grid taking the kinetic energy stored in the rotational masses via the power converters [8]; otherwise, it reduces its active power injection. Consequently, when the frequency speeds up, the wind farm contributes to decelerate the system frequency and, therefore, to reduce the transient angle separations (increasing the transient stability). This control block includes washout and low-pass filters to prevent steady-state action and possible interactions with high-frequency modes. It also presents an output limiter to avoid excessive control excursions. The control parameters are shown in Table 2.

3.2 Remote control block

Wind farms can inject active or reactive powers to achieve the supplementary action for damping inter-area modes [27]. In the considered scheme, the remote control block coordinates the active power delivered by a group of wind farms [6, 28], through measurements from distributed PMUs. The remote control is designed using an observer-based state-feedback approach with transmission time-delay compensation.

The design procedure begins by considering as candidate measurements the bus angle differences among all power plants [29]. Using the geometric approach [16], the set is reduced to signals with a high observability index of the modes of interest (i.e. the low-frequency lightly damped ones, see Table 1), resulting in six angle differences: θ_{futa}–θ_{tand}, θ_{rtur}–θ_{sgde}, θ_{futa}–θ_{rtur}, θ_{yacy}–θ_{tand}, θ_{rtur}–θ_{alic}, and θ_{alic}–θ_{rcor}. The subindex denotes the power plant where the PMU is located. The seven PMUs required to compute these differences are shown with the corresponding symbols in Fig. 1.

To perform the centralised control action, the prioritised wind farms are those presenting both a control input with a high controllability index of the modes of interest and a high rated power. A satisfactory oscillation damping is accomplished by selecting eight wind farms in the Patagonia and Comahue areas, representing 8.5% of the installed power of the system (see the rated power of the wind farms in the Appendix). The selected wind farms (i.e. CERR, 2 × GAST, 2 × PMA, SARA, and 2 × DESE) are indicated by the remote action symbols shown in Fig. 1.

Considering the selected remote measurements (outputs) and wind farms (inputs), a reduced-order model of the Argentine power system is obtained. This can be achieved using either model reduction techniques (e.g. Schur method [30, 31]) or system identification algorithms (e.g. subspace identification [32–34]). In this study, the first approach is used, resulting in an 18th-order reduced model (see details of the methodology in [35]). The reduced model is extended with a time-delay model to consider typical delays in communication channels [36]. In this case, a third-order Padé representation and a time delay of 500 ms are used. A signal conditioning filter is also included (see its cutoff frequencies in Table 2).

Using the reduced model, an optimal linear-quadratic (LQ) control law is calculated. Then, a state observer is designed to estimate the reduced states required by the control law [37, 38]. The weighting matrices to solve the LQ problem in both the control law and the observer designs are included in Table 2. For further details see in [39, 40], where this remote control approach is also applied to the Australian power system and IEEE 50-machine 145-bus system.

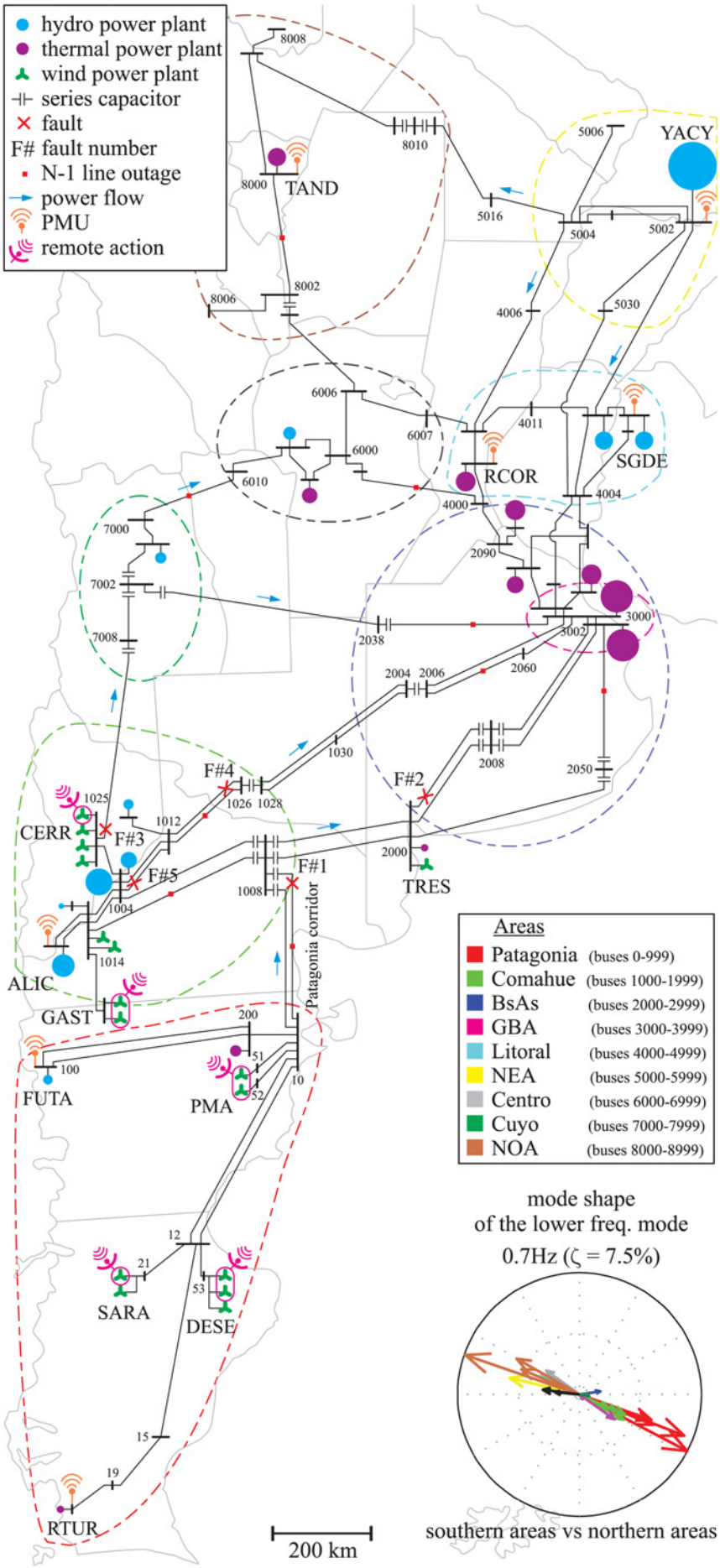

Fig. 1 *Single-line diagram of the case study based on a future scenario of the Argentine power system*

IET Gener. Transm. Distrib., 2016, Vol. 10, Iss. 7, pp. 1622–1633

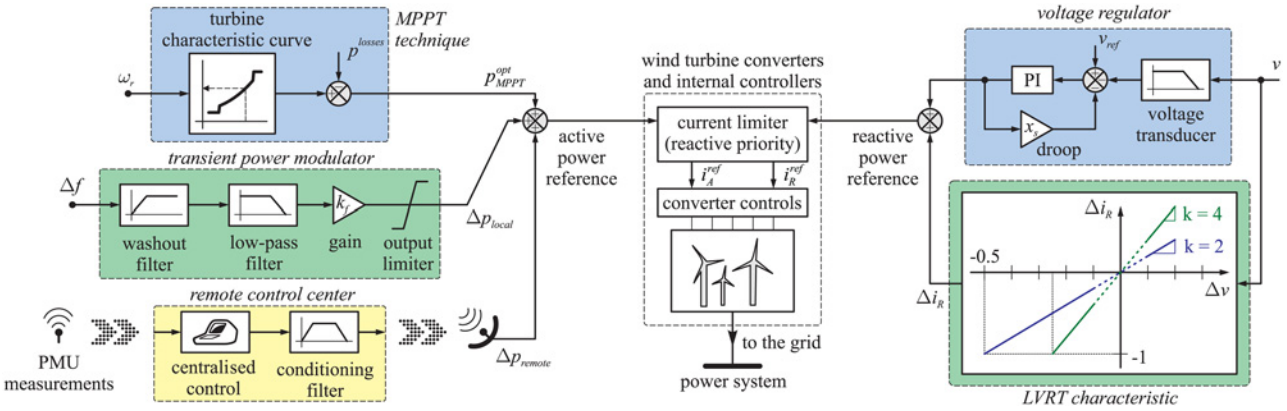

Fig. 2 *Overview of the wind farm controls*

An analogous control design, but in a stochastic approach [linear-quadratic-Gaussian (LQG) control], is also presented in [41].

Note that, in the case of low- or no-wind conditions, the remote control and the TPM will not be able to modulate the turbine active power. However, full-converter wind farms can provide reactive power even when no sufficient wind is available for generating active power [7]. As it will be shown in the following section, the reactive power injection is the main responsible for enhancing the transient stability of the system.

4 Analysis of the dedicated supplementary controls

In this section, the effect of the supplementary controls on the dynamic behaviour of the system is analysed by considering first the individual contribution of each supplementary control block, and then the simultaneous action of the three blocks. With this aim, a three-phase fault is applied at the location F#1 and cleared by opening the faulted line after 120 ms (see the Patagonia corridor in Fig. 1).

The individual results of increasing the reactive slope in the LVRT block, introducing the TPM and considering the remote control action, are presented in the first three columns of Fig. 3, respectively. The fourth column shows the result with the simultaneous contribution of the three supplementary actions. In each case, the system response (denoted in colour curves) is compared with a scenario in which the supplementary controls are not active (denoted in grey curves); that is the wind farms only include the standard MPPT and voltage regulator blocks, and a reactive slope $k = 2$ is used in the LVRT block. To simplify the interpretation, only key variables are shown: the behaviour of the rotor angle of the generator RTUR (located at the farthest point in the south) and the active and reactive powers delivered by the wind farm SARA. All the angles are referred to the centre-of-inertia of the system [21].

The first column of Fig. 3 presents the results when the reactive slope is raised from $k = 2$ to $k = 4$. During the voltage sag, the wind farm reactive power increases, as shown in Fig. 3(c1). This improves the voltage profile, allowing the generator RTUR to export more active power during the fault and, consequently, diminishing its transient rotor angle deviation [compare grey with brown curves in Fig. 3(a1)]. Since the increase of the reactive slope does not practically affect the system eigenvalues, the small-signal response remains unchanged [see Fig. 3(d1)].

The second column shows the effect of the TPM. Immediately after the fault, this control reduces the active power injected by the wind farm, proportionally to the frequency deviation [see Fig. 3 (b2)], collaborating to decelerate the system frequency. Therefore, the transient rotor angle deviations are diminished [compare grey with green curves in Fig. 3(a2)]. In addition, the TPM improves the damping ratio of several eigenvalues [see Fig. 3(d2)].

The third column corresponds to the remote control action. Due to the transmission time delay of the remote measurements, this control action practically does not affect the rotor angles during the first swing. However, the oscillation damping improvement after the first swing is well appreciated in Fig. 3(a3). This is also corroborated by the higher damping ratio of the low-frequency eigenvalues shown in Fig. 3(d3). The power modulation accomplished by the remote control action is illustrated in Fig. 3(b3).

Finally, the fourth column shows the transient and small-signal stability improvement achieved by integrating all the supplementary controls. In this case, the first-swing angle

Table 1 Modal analysis

Mode number	f_n, Hz	ζ, %	Measurement with the highest modal observability	Wind farms with the highest modal controllability
mode #1	0.700	7.5	θ_{futa}–θ_{tand}	CERR, SARA, DESE
mode #2	0.793	9.0	θ_{rtur}–θ_{sgde}	CERR, SARA, PMA
mode #3	0.888	8.8	θ_{futa}–θ_{rtur}	CERR, PMA, GAST
mode #4	0.913	8.6	θ_{yacy}–θ_{tand}	CERR, SARA, DESE
mode #5	0.925	8.0	θ_{rtur}–θ_{alic}	CERR, SARA, GAST
mode #6	0.990	13.5	θ_{alic}–θ_{rcor}	CERR, SARA, PMA

Table 2 Control parameters of the wind farms

Description	Parameter value
MPPT technique	
turbine characteristic curve	extracted from [26]
Voltage regulator	
droop constant (x_s)	5%
proportional\integral gain of the PI regulator	2\1
voltage transducer time constant	0.02 s
LVRT characteristic	
reactive slope k (German grid code)	2
reactive slope k (proposed slope)	4
Transient power modulator (TPM)	
washout\low-pass time constant	10 s\150 ms
gain k_f	33.3
output limiter Δ^{max}_{min}	±0.1 pu
Remote control centre	
lower\upper cutoff frequency of the conditioning filter	0.2\3.5 Hz
transmission time delay	500 ms
reduced-model order	18
weighting matrix of output deviations (control law design)	$15\boldsymbol{I}^{6\times6}$
weighting matrix of control inputs (control law design)	$\boldsymbol{I}^{8\times8}$
weighting matrix of reduced states (observer design)	$500\boldsymbol{I}^{18\times18}$
weighting matrix of measurements (observer design)	$\boldsymbol{I}^{6\times6}$

$\boldsymbol{I}$ is the identity matrix

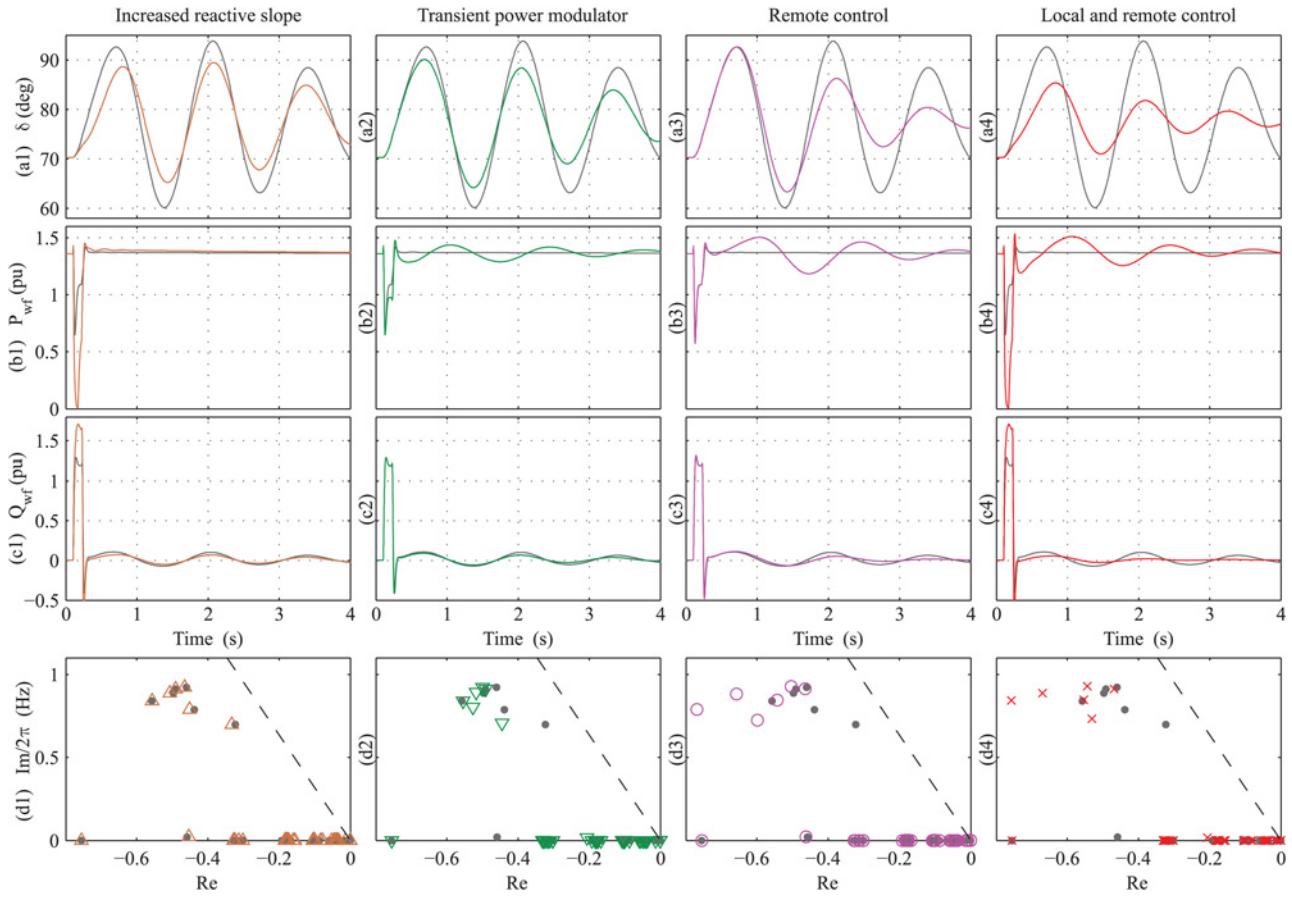

Fig. 3 *Tests considering a three-phase fault at the location F#1 (per-unit values on a 100 MVA base)*

a Rotor angle of the generator RTUR
b, *c* Active and reactive powers delivered by the wind farm SARA
d Eigenvalues of the system with and without the corresponding supplementary control (colour and grey markers, respectively)

deviation is substantially diminished [compare grey with red curves in Fig. 3(a4)]. This is mainly achieved by the increase of the reactive slope and, in a lower proportion, by the TPM. In addition, the damping of the low-frequency electromechanical modes is mostly improved by the remote control action.

5 Transient stability analysis

Additional non-linear time-domain simulations are performed to further evaluate the effect of the supplementary controls on the dynamic behaviour of the system. The scenario including the supplementary controls is compared with a scenario in which the transient stability is enhanced by increasing the series compensation level of the Patagonia corridor from 55 to 70%. These scenarios are denoted in the following as PAT55 and PAT70, respectively. Note that in the scenario PAT70 all the wind farms include the standard controls (dark grey blocks in Fig. 2), but they do not have supplementary actions.

5.1 Faults in corridors exporting wind power from the Patagonia area

These tests are performed to assess the supplementary control actions when faults occur in a corridor which mainly transmits power from wind farms (e.g. the Patagonia corridor, which has a high power ratio between wind generation and conventional generation).

The comparison between the scenarios PAT55 and PAT70 is carried out by applying two different faults at the locations F#1 and F#2 (see fault locations in Fig. 1), and cleared after 120 ms by opening the faulted line. Transient responses of both faults are shown in Fig. 4, where the scenario PAT55 is denoted with black curves, and the scenario PAT70 with grey curves (see the injected powers and the machine names in the figure caption). In the case PAT55 (i.e. when the supplementary controls are included in the wind farms) the maximum transient angle deviations are smaller or equal to that of PAT70 (see Fig. 4*a*). Therefore, to obtain a transient stability improvement such as the one provided by the supplementary controls, the series compensation level in the Patagonia corridor must be increased at least to 70%.

The control actions of the wind farms (active and reactive powers) are shown in Figs. 4*b* and *c*, respectively. The active powers delivered by the wind farms are modified to achieve the stabilising action. This power modulation does not produce a significant change in the turbine speeds, as shown in Fig. 4*d*, where damped torsional modes are also observed. Therefore, the modifications introduced in the control loops do not jeopardise the wind turbine mechanical system. On the other hand, the supplementary control shifts only transiently the turbine speed from the optimal value given by the MPPT, returning to this point in steady state (not shown in Fig. 4*d*).

5.2 Faults in corridors of the Comahue area

In these tests, faults are applied in corridors exporting both wind power and conventional power (mostly hydro generation). Fig. 5 shows the results corresponding to tests consisting in three-phase faults at the locations F#3 and F#4, also cleared after 120 ms by opening the faulted line. Similar conclusions to the previous test are drawn: the transient stability margin of the scenario PAT55 (with the supplementary controls active) is equivalent, or even

IET Gener. Transm. Distrib., 2016, Vol. 10, Iss. 7, pp. 1622–1633

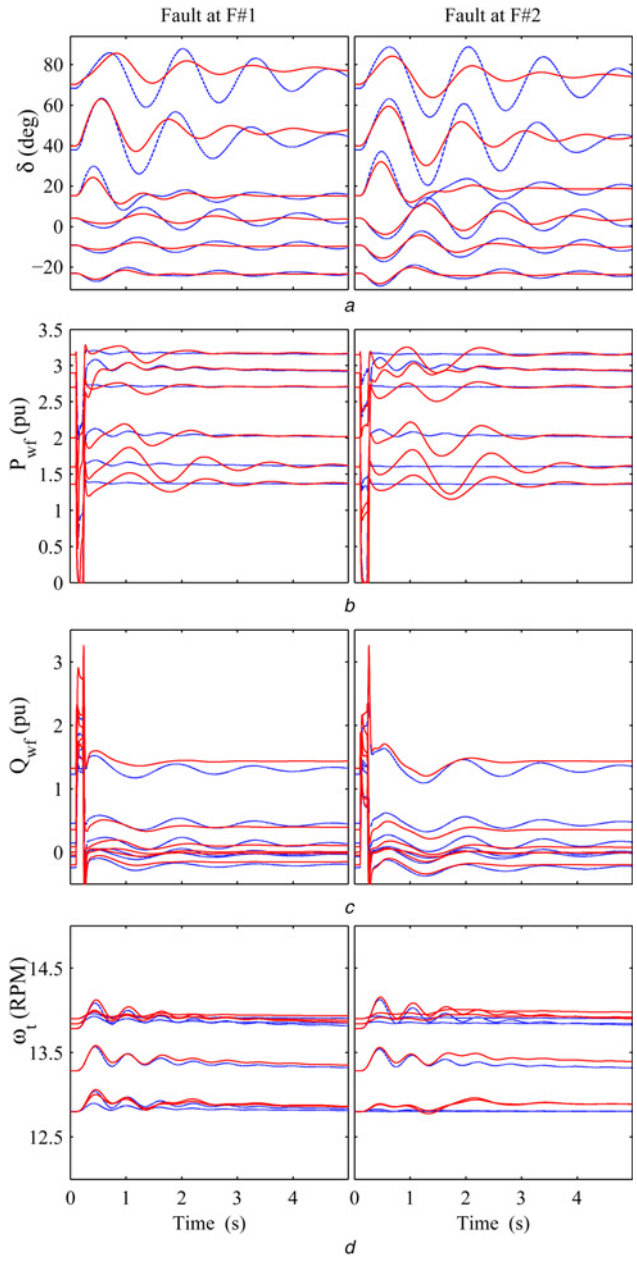

Fig. 4 *Transient responses after faults F#1 and F#2 for the scenarios PAT55 (black curves) and PAT70 (grey curves). Per-unit values on a 100 MVA base*

a Rotor angle of the generators (from top to bottom) RTUR, FUTA, ALIC, TAND, YACY, and SGDE
b, *c* Active and reactive powers delivered by the wind farms DESE, SARA, PMA, CERR, GAST, and TRES
d Wind turbine speeds

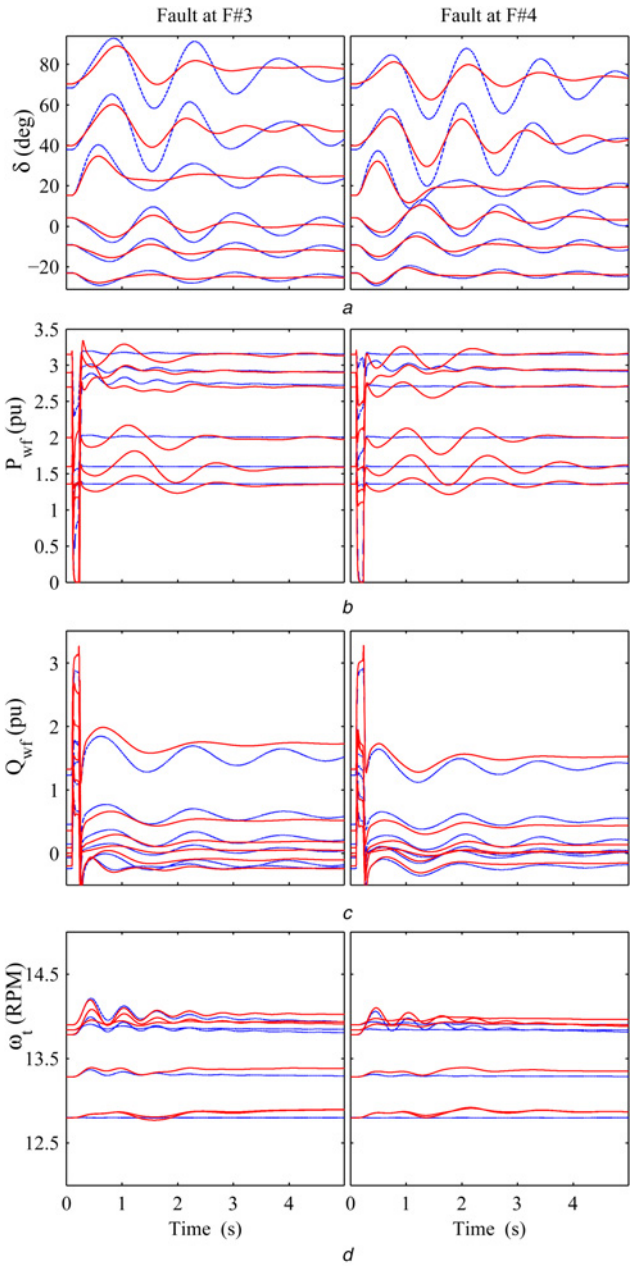

Fig. 5 *Transient responses after faults F#3 and F#4 for the scenarios PAT55 (black curves) and PAT70 (grey curves). Per-unit values on a 100 MVA base*

a Rotor angle of the generators (from top to bottom) RTUR, FUTA, ALIC, TAND, YACY, and SGDE
b, *c* Active and reactive powers delivered by the wind farms DESE, SARA, PMA, CERR, GAST, and TRES
d Wind turbine speeds

better than that of the scenario PAT70, as appreciated by comparing the rotor angle deviations in Fig. 5*a*.

Finally, a more severe test consisting in a fault in the middle of the Comahue area (fault F#5) is performed, but opening the faulted line after 210 ms. The transient responses of the scenarios PAT70 and PAT55 are shown in the first and second columns of Fig. 6, respectively. In this case, the scenario PAT70 is unstable after the disturbance, and the generators of the Patagonia and Comahue areas lose synchronism from the rest of the system (see rotor angles and generator speeds in Figs. 6*a* and *b*, first column). On the other hand, the scenario PAT55 with the action of wind farm supplementary controls maintains all the generators in synchronism (see Fig. 6*a*, second column).

Figs. 6*c* and *d* show the reactive and active currents delivered by the wind farms. In this study, the wind power converters are not over-sized to achieve the supplementary control actions, and their output current is limited to the converter nominal current, prioritising the reactive component. In this way, the converters are protected, and the voltage support is prioritised during fault conditions. In the performed tests, it can be seen that the converters located near the fault reach their maximum current value (see Figs. 6*c* and *d*). When those converters are saturated, the supplementary controls do not provide any additional support. However, the rest of the converters, which do not reach their maximum value, can deliver more reactive current, enhancing the system voltage support. The voltage magnitude of the system buses is shown in Fig. 6*e*. For the case PAT55, in spite of the severe disturbance, all these variables remain within their allowed maximum values, stabilising the system.

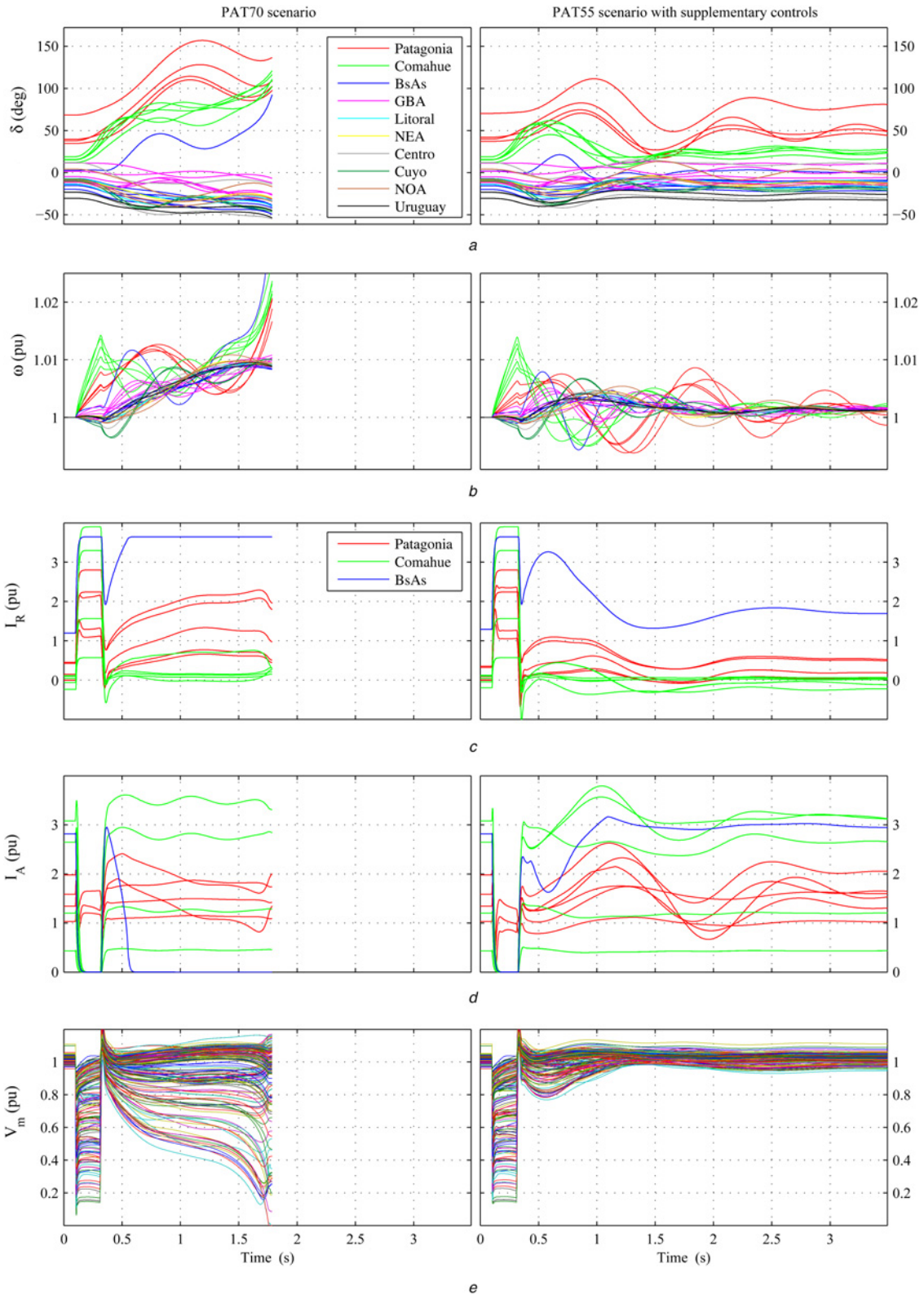

Fig. 6 *Transient responses of the scenarios PAT55 and PAT70 against a 210-ms three-phase fault at F#5. Per unit values on a 100 MVA base*

a, *b* Rotor angles and speeds of the synchronous machines
c, *d* Reactive and active currents delivered by the wind farms
e Voltage magnitude of all the system buses

6 Small-signal stability analysis

This section assesses the impact of the supplementary controls on critical eigenvalues, including intra- and inter-area modes. Fig. 7 shows the eigenvalues corresponding to the scenario PAT55 with local controls only (i.e. using the reactive slope $k = 4$ and the TPM, diamond markers) and to the scenario PAT55 considering both local and remote controls (cross markers). For comparison purposes, the scenario PAT70 is also included (see asterisk markers). The natural frequency and damping ratio of the main

IET Gener. Transm. Distrib., 2016, Vol. 10, Iss. 7, pp. 1622–1633

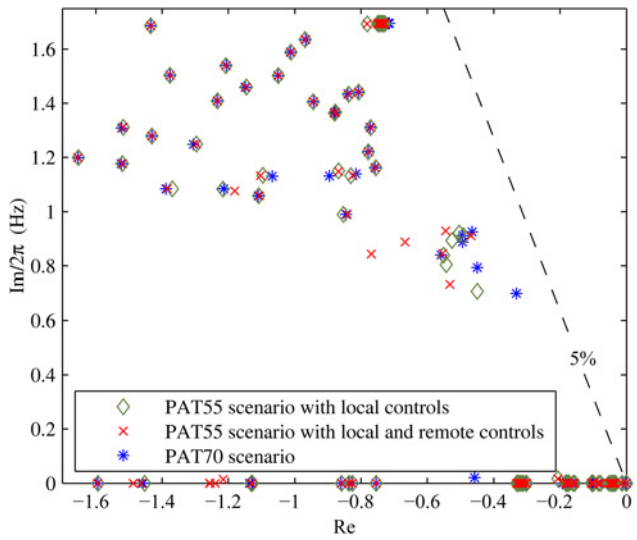

Fig. 7 *Eigenvalue comparison at the nominal operating condition*

Table 3 Impact of the supplementary controls on the main eigenvalues

	Scenario PAT70 without supplementary controls		Scenario PAT55 with local controls only		Scenario PAT55 with local and remote controls	
	f_n, Hz	ζ, %	f_n, Hz	ζ, %	f_n, Hz	ζ, %
mode #1	0.698	7.3	0.708	10.1	0.734	11.5
mode #2	0.787	8.8	0.804	10.7	0.843	14.4
mode #3	0.887	8.9	0.893	9.3	0.887	11.9
mode #4	0.912	8.5	0.911	8.6	0.911	8.5
mode #5	0.922	7.9	0.921	8.7	0.929	9.29
mode #6	0.990	13.4	0.990	13.6	0.990	13.5

eigenvalues for the three considered scenarios are presented in Table 3.

Fig. 7 shows that the local controls are able to improve the damping ratio of the low-frequency modes (below 1 Hz), mainly due to the effect of the TPM [as it was previously shown in Fig. 3 (d2)]. This is important in cases where the centralised control is turned off or the communication link fails. On the other hand, when both local and remote controls are simultaneously operational, a higher damping ratio of the low-frequency modes is observed, and a low impact on the intra-area electromechanical modes (above 1 Hz) is also achieved.

Finally, a robustness evaluation under several changes in the electrical network (e.g. $N-1$ contingencies, daily generation scheduling, and load dispatch) is accomplished to complement the study. Ten different scenarios with $N-1$ line outages on the main corridors are considered (outages are denoted by square symbols in Fig. 1). The apparent power of all load buses is varied ±40% in each scenario, leading to 860 operating conditions. The procedure is performed for the scenario PAT55 (considering the supplementary controls with the nominal tuning) and the scenario PAT70. The eigenvalues corresponding to all the considered cases are shown in Fig. 8, where the scenarios PAT55 and PAT70 are represented by cross and asterisk markers, respectively. The small-signal analysis shows that the wind power converters including supplementary controls are able to significantly and robustly damp the low-frequency modes under different operating conditions, improving the small-signal characteristics obtained by increasing the series compensation level (i.e. scenario PAT70).

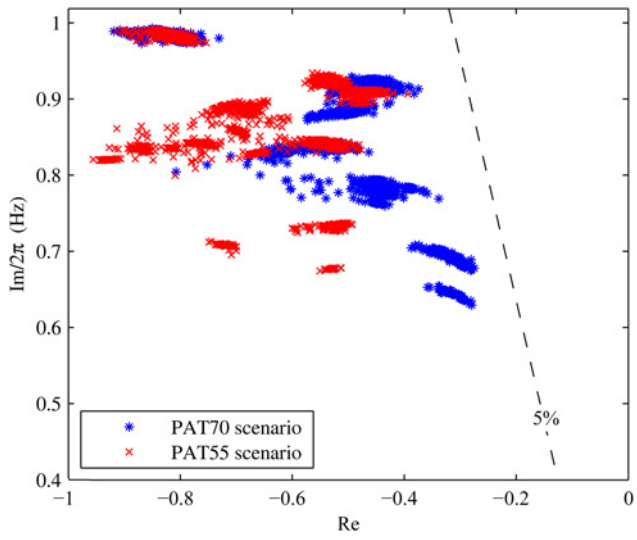

Fig. 8 *Eigenvalues corresponding to all the considered operating conditions. Scenario PAT70 (asterisk markers) and scenario PAT55 with supplementary controls (cross markers)*

7 Conclusions

This work analysed additional grid-support services to improve the stability of power systems with both large-scale wind farms and long-distance transmission lines. The individual and coordinated actions of these supplementary controls using the active and reactive power control loops as well as local and remote measurements were analysed and validated in a practical case study based on the Argentine power system. Specific control modifications in the wind power converters were introduced and tailored to improve the transient and small-signal stability of the system. Local controls resorted to the fast response of the power electronic converters to increase the first-swing stability, whereas a remote control took advantage of the WAMS technology to damp the low-frequency inter-area oscillations.

A comparison was also accomplished between improving the transient stability through either the inclusion of dedicated supplementary controls or the increase of the series compensation level in series-compensated lines exporting a high percentage of wind power. The results obtained from the case study showed that the inclusion of the proposed auxiliary signals in the wind turbine controls enables a transient stability improvement equivalent to the one obtained by increasing the series compensation level from 55 to 70% in the Patagonia corridor.

Furthermore, the wind farm supporting tasks enabled to maximise the use of the existing facilities, to enhance the power system operation and to minimise the blackout probabilities. In the near future, as the penetration levels of wind energy conversion systems grow, this kind of control approaches which take advantage of modern power converters and WAMS technologies will become more common.

8 References

1 Gautam, D., Goel, L., Ayyanar, R., *et al.*: 'Control strategy to mitigate the impact of reduced inertia due to doubly fed induction generators on large power systems', *IEEE Trans. Power Syst.*, 2011, **26**, (1), pp. 214–224

2 Nguyen, M.H., Saha, T.K., Eghbal, M.: 'Input/output selection for wide-area power oscillation damper of hybrid multi-terminal high-voltage direct current to connect remotely located renewable energy resources', *IET Gener. Transm. Distrib.*, 2015, **9**, (5), pp. 483–493

3 Larsen, E.V.: 'Wind generators and series-compensated AC transmission lines'. IEEE PES Transmission and Distribution Conf. and Exposition, 2012, pp. 1–4

4 Revel, G., Leon, A.E., Alonso, D.M., *et al.*: 'Dynamics and stability analysis of a power system with a PMSG-based wind farm performing ancillary services', *IEEE Trans. Circuits Syst. I, Regul. Pap.*, 2014, **61**, (7), pp. 2182–2193

5 Ullah, N.R., Thiringer, T., Karlsson, D.: 'Voltage and transient stability support by wind farms complying with the E.ON Netz Grid Code', *IEEE Trans. Power Syst.*, 2007, **22**, (4), pp. 1647–1656

6 Tsourakis, G., Nomikos, B.M., Vournas, C.D.: 'Contribution of doubly fed wind generators to oscillation damping', *IEEE Trans. Energy Convers.*, 2009, **24**, (3), pp. 783–791
7 Wachtel, S., Hartge, S.: 'Technical and economical benefits of wind energy converters with FACTS capabilities for power system and the grid integration of wind power'. EWEC Conf., May 2007, pp. 1–8
8 Hughes, F.M., Anaya-Lara, O., Jenkins, N., *et al.*: 'Control of DFIG-based wind generation for power network support', *IEEE Trans. Power Syst.*, 2005, **20**, (4), pp. 1958–1966
9 Grunbaum, R., Ingestrom, G., Ekehov, B., *et al.*: '765 kV series capacitors for increasing power transmission capacity to the Cape Region'. IEEE Power Engineering Society Conf. and Exposition, July 2012, pp. 1–8
10 ABB technical publication. Series compensation: Boosting transmission capacity. www.abb.com/FACTS, December 2010, pp. 1–16
11 Daniel, J., Han, C., Hutchinson, S., *et al.*: 'ERCOT CREZ reactive power compensation study'. Report No.: E3800-PR-00, ABB Inc., Power Systems Division, Grid Systems Consulting, 2010
12 Mohammadpour, H.A., Ghaderi, A., Santi, E.: 'Analysis of sub-synchronous resonance in doubly-fed induction generator-based wind farms interfaced with gate-controlled series capacitor', *IET Gener. Transm. Distrib.*, 2014, **8**, (12), pp. 1998–2011
13 Leon, A.E., Mauricio, J.M., Solsona, J.A.: 'Subsynchronous resonance mitigation using variable-speed wind energy conversion systems', *IET Gener. Transm. Distrib.*, 2013, **7**, (5), pp. 511–525
14 Livermore, L., Ugalde-Loo, C.E., Mu, Q., *et al.*: 'Damping of subsynchronous resonance using a voltage source converter-based high-voltage direct-current link in a series-compensated Great Britain transmission network', *IET Gener. Transm. Distrib.*, 2014, **8**, (3), pp. 542–551
15 Leon, A.E., Solsona, J.A.: 'Sub-synchronous interaction damping control for DFIG wind turbines', *IEEE Trans. Power Syst.*, 2015, **30**, (1), pp. 419–428
16 Zhang, Y., Bose, A.: 'Design of wide-area damping controllers for interarea oscillations', *IEEE Trans. Power Syst.*, 2008, **23**, (3), pp. 1136–1143
17 Taylor, C.W., Erickson, D.C., Martin, K.E., *et al.*: 'WACS–Wide-area stability and voltage control system: R&D and online demonstration', *Proc. IEEE*, 2005, **93**, (5), pp. 892–906
18 Zhu, K., Nordström, L.: 'Design of wide-area damping systems based on the capabilities of the supporting information communication technology infrastructure', *IET Gener. Transm. Distrib.*, 2014, **8**, (4), pp. 640–650
19 Chaudhuri, N.R., Chaudhuri, B., Ray, S., *et al.*: 'Wide-area phasor power oscillation damping controller: a new approach to handling time-varying signal latency', *IET Gener. Transm. Distrib.*, 2010, **4**, (5), pp. 620–630
20 Samuelsson, J.O., Wilk-Wilczynski, A.L., Nizovoy, J.A.: 'Increase of transmission capacity by resource pooling in Argentina'. Power Engineering Society Summer Meeting, 2001, vol. 1, pp. 38–42
21 Kundur, P.: 'Power system stability and control' (McGraw-Hill, 1994)
22 Clark, K., Miller, N.W., Sanchez-Gasca, J.J.: 'Modeling of GE wind turbine-generators for grid studies, Version 4.5' (General Electric International, Inc., Schenectady, New York, 2010)
23 Nanou, S., Tsourakis, G., Vournas, C.D.: 'Full-converter wind generator modelling for transient stability studies'. IEEE Trondheim PowerTech, June 2011, pp. 1–7
24 Martinez, J., Kjar, P.C., Rodriguez, P., *et al.*: 'Comparison of two voltage control strategies for a wind power plant'. IEEE/PES Power Systems Conf. and Exposition, March 2011, pp. 1–9
25 E.ON Netz GmbH. Grid Code for high and extra high voltage. *Grid Connection Regulations*, April 2006, pp. 1–46. www.eon-netz.com
26 Slootweg, J.G., de Haan, S.W.H., Polinder, H., *et al.*: 'General model for representing variable speed wind turbines in power system dynamics simulations', *IEEE Trans. Power Syst.*, 2003, **18**, (1), pp. 144–151
27 Morato, J., Knuppel, T., Ostergaard, J.: 'Residue-based evaluation of the use of wind power plants with full converter wind turbines for power oscillation damping control', *IEEE Trans. Sustain. Energy*, 2014, **5**, (1), pp. 82–89
28 Knuppel, T., Nielsen, J.N., Jensen, K.H., *et al.*: 'Power oscillation damping controller for wind power plant utilizing wind turbine inertia as energy storage'. IEEE Power and Energy Society General Meeting, 2011, pp. 1–8
29 Chaudhuri, N.R., Domahidi, A., Majumder, R., *et al.*: 'Wide-area power oscillation damping control in nordic equivalent system', *IET Gener. Transm Distrib*, 2010, **4**, (10), pp. 1139–1150
30 Ke, D.P., Chung, C.Y., Xue, Y.: 'An eigenstructure-based performance index and its application to control design for damping inter-area oscillations in power systems', *IEEE Trans. Power Syst.*, 2011, **26**, (4), pp. 2371–2380
31 Yao, W., Jiang, L., Wen, J., *et al.*: 'Wide-area damping controller of FACTS devices for inter-area oscillations considering communication time delays', *IEEE Trans. Power Syst.*, 2014, **29**, (1), pp. 318–329
32 Zhang, P., Yang, D.Y., Chan, K.W., *et al.*: 'Adaptive wide-area damping control scheme with stochastic subspace identification and signal time delay compensation', *IET Gener. Transm. Distrib.*, 2012, **6**, (9), pp. 844–852
33 Zhou, N., Pierre, J.W., Hauer, J.F.: 'Initial results in power system identification from injected probing signals using a subspace method', *IEEE Trans. Power Syst.*, 2006, **21**, (3), pp. 1296–1302
34 Eriksson, R., Soder, L.: 'Wide-area measurement system-based subspace identification for obtaining linear models to centrally coordinate controllable devices', *IEEE Trans. Power Deliv.*, 2011, **26**, (2), pp. 988–997
35 Safonov, M.G., Chiang, R.Y.: 'A Schur method for balanced-truncation model reduction', *IEEE Trans. Autom. Control*, 1989, **34**, (7), pp. 729–733
36 Zhang, S., Vittal, V.: 'Design of wide-area power system damping controllers resilient to communication failures', *IEEE Trans. Power Syst.*, 2013, **28**, (4), pp. 4292–4300
37 Ogata, K.: 'Modern control engineering' (Prentice-Hall, 1997)
38 Li, Y., Rehtanz, C., Yang, D., *et al.*: 'Robust high-voltage direct current stabilising control using wide-area measurement and taking transmission time delay into consideration', *IET Gener. Transm. Distrib.*, 2011, **5**, (3), pp. 289–297
39 Pipelzadeh, Y., Chaudhuri, B., Green, T.C.: 'Wide-area power oscillation damping control through HVDC: A case study on Australian equivalent system'. IEEE Power and Energy Society Meeting, 2010, pp. 1–7
40 Leon, A.E., Solsona, J.A.: 'Power oscillation damping improvement by adding multiple wind farms to wide-area coordinating controls', *IEEE Trans. Power Syst.*, 2014, **29**, (3), pp. 1356–1364
41 Preece, R., Milanovic, J.V., Almutairi, A.M., *et al.*: 'Probabilistic evaluation of damping controller in networks with multiple VSC-HVDC lines', *IEEE Trans. Power Syst.*, 2013, **28**, (1), pp. 367–376

9 Appendix

The relevant data corresponding to the transmission lines, synchronous generators, wind farms and loads used in the case study are shown in Tables 4–7, respectively. The power flow of the most representative transmission lines is included in the last column of Table 4, where the lines are grouped considering the main corridors of the system. Note that the bus numbers of the different lines and power plants are arranged according to the areas of the power system (see the numeration range for each area in Fig. 1). Finally, the voltage profile of the system is also presented in Fig. 9.

Table 4 Line data

#	Initial node	Final node	*R*	*X*	*B*	μ, %	Longitude, km	Power flow, MW
	19	15	0.00135	0.01625	1.9579	–	167	182.4
	15	12	0.00302	0.03725	4.6508	–	392	151.7
	21	12	0.00105	0.01268	1.5225	–	123	239.4
	53	12	0.00012	0.00146	0.1754	–	14	479.7
2×	12	10	0.00401	0.05098	6.6528	–	552.5	427.9
	51	10	0.00008	0.00099	0.1161	–	10	200.0
	52	10	0.00008	0.00099	0.1161	–	10	160.0
2×	100	200	0.02333	0.16818	2.0808	–	550	220.0
2×	10	1008	0.00275	0.03384	4.1888	55.0	354	757.1
2×	1000	1012	0.00093	0.01000	0.9340	–	90	993.2
2×	1012	1026	0.00217	0.02358	2.2306	–	214	1114
	1026	1028	0.00000	−0.01162	0.0000	–	–	2179
	1028	2004	0.00406	0.04524	4.4449	–	421	1068
	1028	1030	0.00230	0.02499	2.3674	–	227	1110
	1030	2004	0.00198	0.02141	2.0206	–	194	962.8
	2004	2006	0.00000	−0.01162	0.0000	–	–	1968
	2006	3000	0.00312	0.03415	3.2791	–	313	735.0
	2006	2060	0.00162	0.01748	1.6436	–	162	914.4
	2060	3000	0.00159	0.01715	1.6122	–	159	546.4
2×	1004	1000	0.00003	0.00039	0.0365	–	4.5	423.3
	1004	1008	0.00244	0.02960	2.8289	58.6	269	341.0
	1014	1004	0.00151	0.01821	1.7181	–	165	730.8
	1014	1004	0.00152	0.01825	1.7213	–	170	729.1
	1014	1008	0.00293	0.03612	4.6688	40.4	387	782.6
	1008	2000	0.00308	0.03772	3.6557	46.8	348	1256
	1008	2000	0.00267	0.03272	4.1949	42.5	346	1347
	2000	2008	0.00232	0.02810	2.6797	49.6	255	917.8
	2000	2008	0.00200	0.02419	3.0511	40.3	255	920.7
	2008	3002	0.00263	0.03194	3.0640	47.8	302	709.8
	2008	3002	0.00234	0.02852	3.6241	46.0	291	763.3
	3002	3000	0.00059	0.00650	0.6022	–	58	605.9
	3002	3000	0.00057	0.00654	0.5981	–	58	602.6
	2000	2050	0.00306	0.03799	4.7491	55.0	372	958.9
	2050	3002	0.00279	0.03439	4.2616	55.0	336	490.2
	1004	1025	0.00041	0.00500	0.6187	–	52	844.7
	1025	7008	0.00212	0.02567	3.1074	70.0	250	1417
	7008	7002	0.00204	0.02463	2.9768	70.0	240	1340
	7002	2038	0.00381	0.04772	6.1569	35.0	472	810.5
	2038	3001	0.00293	0.03581	4.4591	70.0	351	642.5
	3000	3001	0.00026	0.00283	0.2572	–	26	325.2
	3000	3001	0.00023	0.00237	0.2470	–	23	387.7

Parameters are in p.u. on a 100 MVA base

Table 5 Synchronous generator data

Bus number	Generator name	Rated power, MVA
102	FUTA-HI	472
190	AL-TGCC	369
192	AL-TVCC	190.8
523	RTUR-TV	290
1611	ALIC-HI	1120
1656	CHIUI-HI	800
1661	CHOC-HI01-2	444
1663	CHOC-HI03-4	444
1665	CHOC-HI05-6	444
1681	PPLE-HI	270
1691	PBAN-HI	500
2620	ATUC-NU	838
2629	BBLA-TV	364.7
2692	S.NIC-G	618
2694	S.NIC-V	375.6
2695	BELGR-TG	612
2697	BELGR-TV	375.6
3641	GEBA-TG01	460
3643	GEBA-CV03	261
3647	GEBA-TG04	195
3900	ABA	2000
3913	EZE	2000
3919	ROD	2000
4601	SGDE-HI01-2	300
4603	SGDE-HI03-4	300
4605	SGDE-HI05-6	300
4695	TIMB-TG	602
4697	TIMB-TV	375.6
5671	YACY-HI	3277.5
6600	EMBA-NUCL	763.5
6671	RGDE-HB01-2	420
6673	RGDE-HB03	210
7626	LBCO1-HI	412.5
7629	LBCO2-HI	143
8614	SMTU-TG	164.7
8615	SMTU-TV	194.1
8622	TAND-ESG	540
98,011	SGDE-HI07-8	300
98,013	SGDE-HI09-10	300
98,015	SGDE-HI11-12	300
98,511	PAL1	111
98,512	PAL2	111
98,513	PAL3	111

Table 6 Wind farm data

Bus number	Wind farm name	Rated power, MVA
561	PMA1[a]	280
562	PMA2[a]	224
621	SARA1	162.5
622	SARA2[a]	212.5
974	DES1[a]	250
975	DES2[a]	250
976	DES3	250
1600	CERR1	156.47
1602	CERR2	56.76
1603	CERR3	56.76
1604	CERR4	56.76
1605	CERR5	56.76
1606	CERR6[a]	330
1651	GAST1[a]	390
1652	GAST2[a]	390
1653	GAST3	390
1654	GAST4	390
2630	TRES	364.7

[a]Wind farms with remote control actions

Table 7 Load data

Bus number	Bus name	*P*, MW	*Q*, MVA
15	RIOSCRUZ	30.00	9.860
117	ESPERANZ	60.00	19.72
261	AL-CEA	580.0	190.6
1016	ALICURA	122.0	40.09
1024	P.BAND.	167.0	54.89
1030	MACACHIN	120.0	39.44
2000	B.BLANCA	290.0	95.31
2002	CAMPANA	454.0	149.2
2006	HENDERS2	319.0	104.8
2008	OLAVARRI	328.0	107.8
2040	VILLEGAS	168.0	55.21
2050	M.PLATA	440.0	144.6
2060	25MAYO	355.0	116.6
2090	RAMALLO	374.0	122.9
3000	EZEIZA	4340	1426
3002	ABASTO	2020	663.9
3004	RODRGUEZ	3200	1051
3014	O.SMITH	1375	451.9
4000	R.OESTE	1119	367.7
4002	R.COROND	280.0	92.03
4004	C.ELIA	214.0	70.33
4006	ROMANG	220.0	72.31
4008	SGDE.ARG	210.0	69.02
4010	S.TOME	230.0	75.59
4011	G.PARANA	270.0	88.74
5000	YACYRETA	100.0	32.86
5002	RINCON	65.0	21.36
5004	RESISTEN	379.0	124.5
5005	P.PATRIA	310.0	101.8
5006	GRANFORMOSA	210.0	69.02
5016	CHACO	198.0	65.07
5030	MERCEDES	146.0	47.98
5253	S.ISIDRO	261.0	85.78
6000	ALMAFUE	259.0	85.12
6002	A.CABRAL	135.0	44.37
6006	MALVINAS	512.0	168.2
6007	SFRANSCO	150.0	49.30
6010	LUJAN.SL	204.0	67.05
7000	GRANMZA	420.0	138.0
8000	BRACHO	251.0	82.49
8002	RECREO	213.0	70.00
8006	RIOJASUR	144.0	47.33
8008	JUANCITO	41.0	13.47
8010	MQUEMADO	82.0	26.95
8120	COBOS	171.0	56.20

IET Gener. Transm. Distrib., 2016, Vol. 10, Iss. 7, pp. 1622–1633

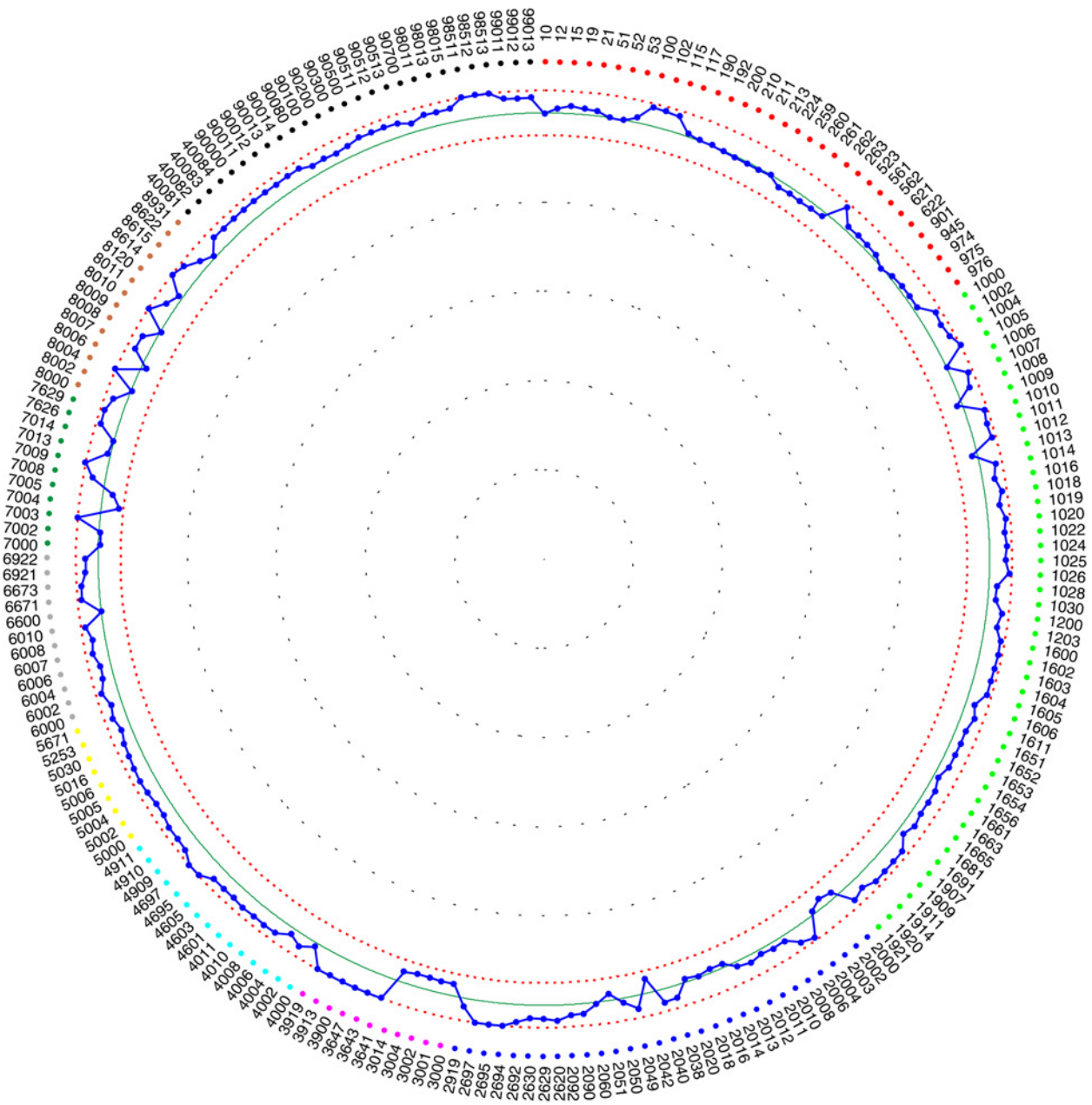

Fig. 9 *Voltage profile of the system buses (solid curve), zone with a tolerance of ±5% (dotted curve), and line with unity voltage*